AD-A057 292 DAVID W TAYLOR NAVAL SHIP RESEARCH AND DEVELOPMENT CE--ETC F/G 13/7
DYNAMIC RESPONSE OF LIFT FANS SUBJECT TO VARYING BACKPRESSURE.(U)
JUL 78 J M DURKIN, L H LUEHR

UNCLASSIFIED AERO-1253 DTNSRDC-78/063 NL

1 OF 1
AD
A057 292

END
DATE
FILMED
9-78
DDC

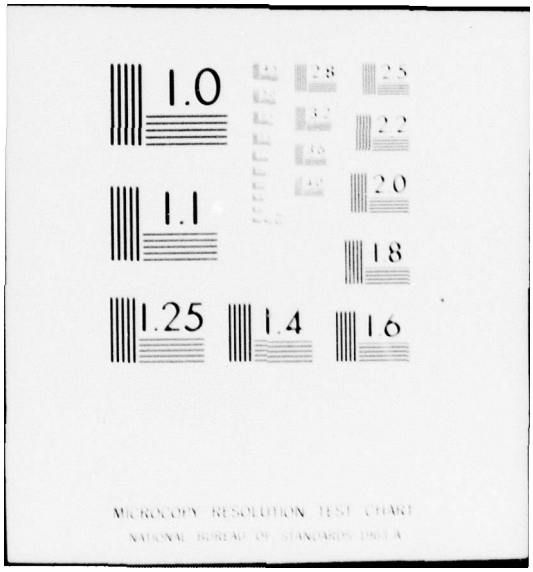
1.0
1.1
1.25
1.4
1.6
2.8
2.5
2.2
2.0
1.8
MICROCOPY RESOLUTION TEST CHART
NATIONAL BUREAU OF STANDARDS 1963-A

# DAVID W. TAYLOR NAVAL SHIP RESEARCH AND DEVELOPMENT CENTER

Bethesda, Maryland 20084

(6) DYNAMIC RESPONSE OF LIFT FANS SUBJECT TO VARYING BACKPRESSURE

by

(10) John M. Durkin
Lawrence H. Luehr



APPROVED FOR PUBLIC RELEASE: DISTRIBUTION UNLIMITED

Reprinted from AIAA Paper 78-756

(14) AERO-1253

AVIATION AND SURFACE EFFECTS DEPARTMENT

(9) RESEARCH AND DEVELOPMENT REPORT

(16) SØ3Ø8 (17) SØ3Ø8ØØ1

(12) 18p.

(19)

(11) July 1978 (18) DTNSRDC/78/063

DYNAMIC RESPONSE OF LIFT

## MAJOR DTNSRDC ORGANIZATIONAL COMPONENTS

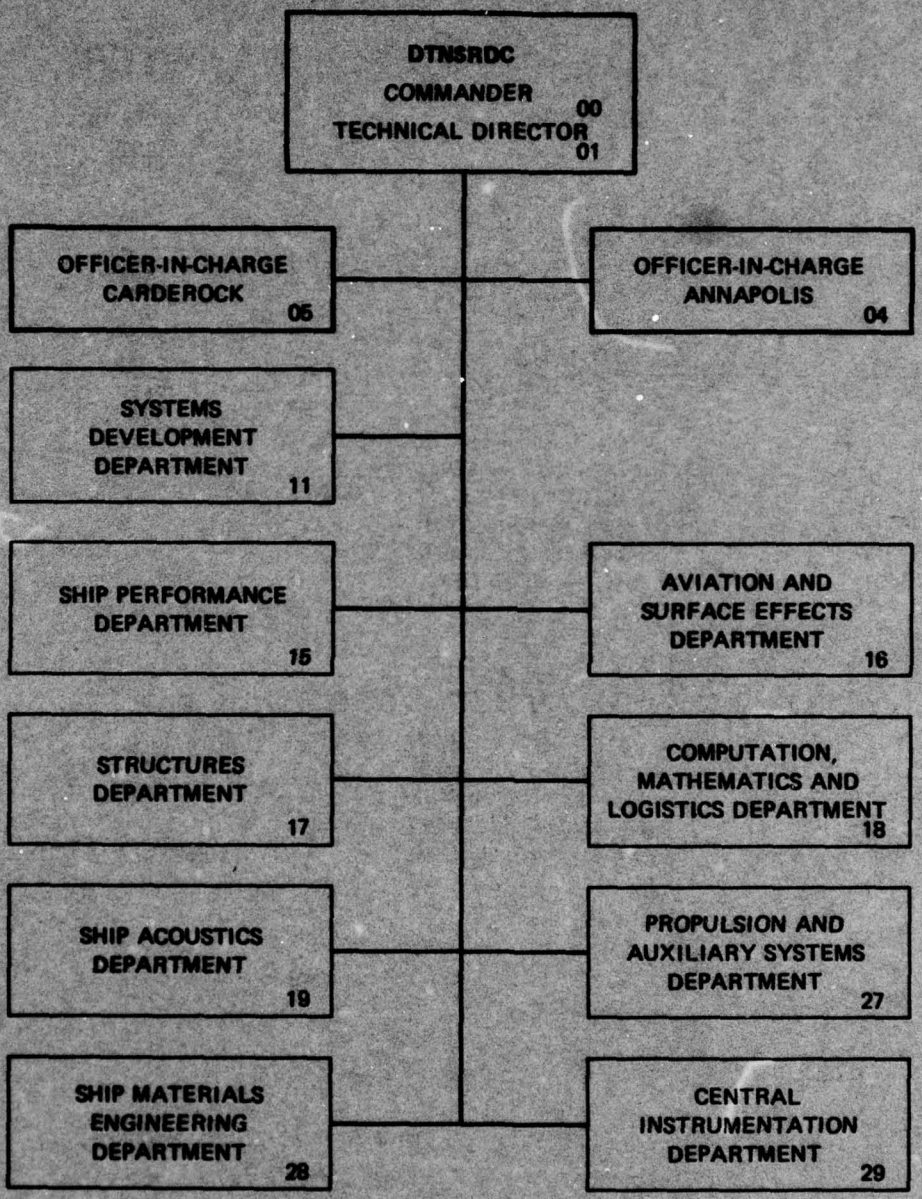


NDW-DTNSRDC 3960/43b (Rev. 3-78)
GPO 928 740

UNCLASSIFIED

SECURITY CLASSIFICATION OF THIS PAGE (When Data Entered)

| REPORT DOCUMENTATION PAGE | | READ INSTRUCTIONS BEFORE COMPLETING FORM |
|---|---|---|
| 1. REPORT NUMBER<br>DTNSRDC-78/063 | 2. GOVT ACCESSION NO. | 3. RECIPIENT'S CATALOG NUMBER |
| 4. TITLE (and Subtitle)<br>DYNAMIC RESPONSE OF LIFT FANS SUBJECT TO VARYING BACKPRESSURE | | 5. TYPE OF REPORT & PERIOD COVERED<br>6. PERFORMING ORG. REPORT NUMBER<br>Aero Report 1253 |
| 7. AUTHOR(s)<br>John M. Durkin and Lawrence H. Luehr | | 8. CONTRACT OR GRANT NUMBER(s) |
| 9. PERFORMING ORGANIZATION NAME AND ADDRESS<br>David W. Taylor Naval Ship R&D Center<br>Aviation and Surface Effects Department<br>Bethesda, Maryland 20084 | | 10. PROGRAM ELEMENT, PROJECT, TASK AREA & WORK UNIT NUMBERS<br>(See reverse side) |
| 11. CONTROLLING OFFICE NAME AND ADDRESS<br>Naval Sea Systems Command<br>Surface Effect Ships Project Office (PMS-304)<br>Bethesda, Maryland 20084 | | 12. REPORT DATE<br>July 1978<br>13. NUMBER OF PAGES<br>17 |
| 14. MONITORING AGENCY NAME & ADDRESS(if different from Controlling Office) | | 15. SECURITY CLASS. (of this report)<br>UNCLASSIFIED<br>15a. DECLASSIFICATION/DOWNGRADING SCHEDULE |

16. DISTRIBUTION STATEMENT (of this Report)

APPROVED FOR PUBLIC RELEASE: DISTRIBUTION UNLIMITED

17. DISTRIBUTION STATEMENT (of the abstract entered in Block 20, if different from Report)

18. SUPPLEMENTARY NOTES

Presented at the AIAA/SNAME Advanced Marine Vehicles Conference, San Diego, California, 17-19 April 1978. AIAA Paper 78-756. Lawrence H. Luehr is employed by Aerojet Liquid Rocket Co., Sacramento, California.

19. KEY WORDS (Continue on reverse side if necessary and identify by block number)

Lift Fans
Lift Fan Dynamic Performance
Lift Fan Unsteady Effects
Fan Inertance
Fan Capacitance

20. ABSTRACT (Continue on reverse side if necessary and identify by block number)

An analytical investigation of the dynamic performance of a centrifugal lift fan was conducted to provide an explanation for the behavior which occurred when the fan was subjected to a varying backpressure. Analysis of test data shows that the fan response $\delta Q/\delta P$ can be represented by a first-order lag system. An in-depth analysis of the various elements of the lift fan system revealed that the inertia of the air within the fan was the

(Continued on reverse side)

DD FORM 1 JAN 73 1473 EDITION OF 1 NOV 65 IS OBSOLETE
S/N 0102-LF-014-6601

UNCLASSIFIED

SECURITY CLASSIFICATION OF THIS PAGE (When Data Entered)

(Block 10)

Task Area SO 308 001
Program Element 63534N
Work Unit 1-1630-050

(Block 20 continued)

primary contributor to the observed fan behavior. The analysis further showed that variations in fan speed would not produce the behavior measured in the test and that the response due to the compliant properties of air within the fan occurs at a frequency that is much higher than the frequency range of the test. A time-domain digital computer program has been developed which integrates the rate of change of fan flow with a varying backpressure. Good correlation is exhibited between test data and the computer predictions at all frequencies.

TABLE OF CONTENTS



LIST OF FIGURES

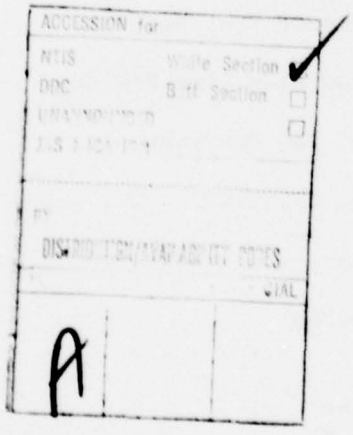

# DYNAMIC RESPONSE OF LIFT FANS SUBJECT TO VARYING BACKPRESSURE

John M. Durkin, Aerospace Engineer
Aviation and Surface Effects Department
David W. Taylor Naval Ship Research and Development Center
Bethesda, Maryland 20084
and
Lawrence H. Luehr, Engineering Specialist
Aerojet Liquid Rocket Co.
Sacramento, California 95813

## Abstract

An analytical investigation of the dynamic performance of a centrifugal lift fan was conducted to provide an explanation for the behavior which occurred when the fan was subjected to a varying backpressure. Analysis of test data shows that the fan response $\delta Q/\delta P$ can be represented by a first-order lag system. An in-depth analysis of the various elements of the lift fan system revealed that the inertia of the air within the fan was the primary contributor to the observed fan behavior. The analysis further showed that variations in fan speed would not produce the behavior measured in the test and that the response due to the compliant properties of air within the fan occurs at a frequency that is much higher than the frequency range of the test. A time-domain digital computer program has been developed which integrates the rate of change of fan flow with a varying backpressure. Good correlation is exhibited between test data and the computer predictions at all frequencies.

## Nomenclature

| | |
|---|---|
| A | Area of flow channel, $ft^2$ |
| $A_i$ | Area of $i^{th}$ section of plenum wall, $ft^2$ |
| C | Compliance of air in fan, $ft^5/lb$ |
| $C_D$ | Discharge coefficient |
| $F_2$ | Inverse of fan characteristic slope, $ft^3/s/lb/ft^2$ |
| f | Frequency, Hz |
| I | Inertia of rotating system, ft-lbf/$s^2$ |
| j | $(-1)^{1/2}$ |
| L | Inertance of air in fan, lb-$s^2/ft^5$ |
| m | Mass of air in the fan, lbm-$s^2/ft$ |
| N | Shaft rotational speed, rpm |
| P | Pressure, $lb/ft^2$ |
| Q | Fan flow rate, $ft^3/s$ |
| $Q_L$ | Uncontrolled plenum flow due to leakage, $ft^3/s$ |
| $Q_P$ | Controlled flow from plenum, $ft^3/s$ |
| S | Distance along flow path, ft |
| T | Torque, lbf-ft |
| t | Time, s |
| $V_P$ | Plenum volume, $ft^3$ |
| V | Velocity, ft/s |
| $Z_i$ | Deflection of $i^{th}$ section of plenum wall, ft |
| $\rho$ | Mass density, lbm-$s^2/ft^4$ |
| $\omega$ | Rotational velocity, rad/s |

### Subscripts

| | |
|---|---|
| ATM | Ambient conditions |
| c | Corner |
| F | Fan |
| I | Inlet |
| L | Leakage |
| M | Motor |
| P | Plenum |
| S | Static |
| T | Total |



## Introduction

In Surface Effect Ships (SES) and Air Cushion Vehicles (ACV), the lift fan characteristic pressure versus flow rate curve is known to have a significant effect on the vertical motions of the platform. Exposure of the crew to adverse motions results in degraded human performance and reduced overall system effectiveness.[1] Analysis techniques to predict the motions of SES and ACVs span the spectrum from simple, linear, single degree-of-freedom models to elaborate, time-domain, multi-degree-of-freedom models. In all cases, the primary vertical force arises from the cushion pressure acting on the wet deck. The cushion pressure is derived in these analytical models by integrating the time rate of change of the mass of air in the cushion plenum which in turn is determined using the conservation of mass equation. The rate at which air is delivered from the fans to the plenum is usually determined using the steady state fan characteristic in the form $Q = f(p)$. This assumes that the fan behavior is the same under steady-state and dynamic conditions.

In order to investigate the behavior of lift fans in unsteady flow conditions, a test rig was constructed at the David W. Taylor Naval Ship Research and Development Center (DTNSRDC). This lift fan evaluation rig features an 820 $ft^3$ plenum and an exhaust duct containing a flow control valve (Fig. 1).

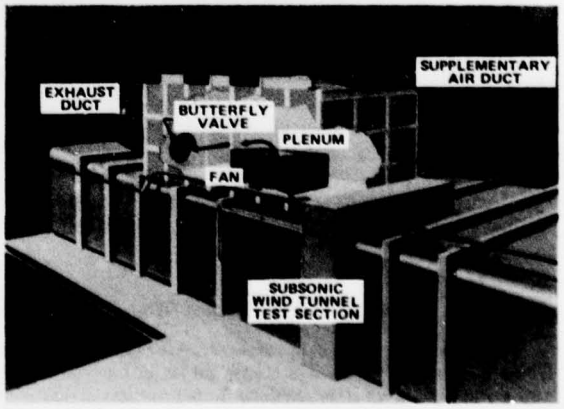


Fig. 1 – Artist's Sketch of the Fan Evaluation Rig

The fan delivers pressurized air into the plenum. Appropriate instrumentation is located at the fan inlet and discharge to measure the flow rate and pressure rise across the fan. An evaluation was conducted using a 24-in. diameter model of the SES-100B cushion fan, representative of high-efficiency backward swept airfoil (HEBA) centrifugal fans. Data from this evaluation showed that under dynamic conditions, the flow rate change lagged the pressure change in such a manner that the pressure versus flow rate characteristic no longer followed the steady state curve but instead, when plotted on the standard pressure versus flow rate plot, exhibited loops.[2] Fig. 2 presents examples of the pressure versus flow rate loops that were obtained during the evaluation of the SES-100B scale model cushion fan. These loops are superimposed on the steady state fan characteristic. The data show the variation of the loop shape with the frequency of the back pressure change. They also illustrate the steepening of the effective slope of the fan characteristic (determined by the orientation of the major axis of the "ellipse" formed by the loop) as the frequency is increased. A lift system designer could rightfully ask what fan characteristic should be selected for typical dynamic conditions.

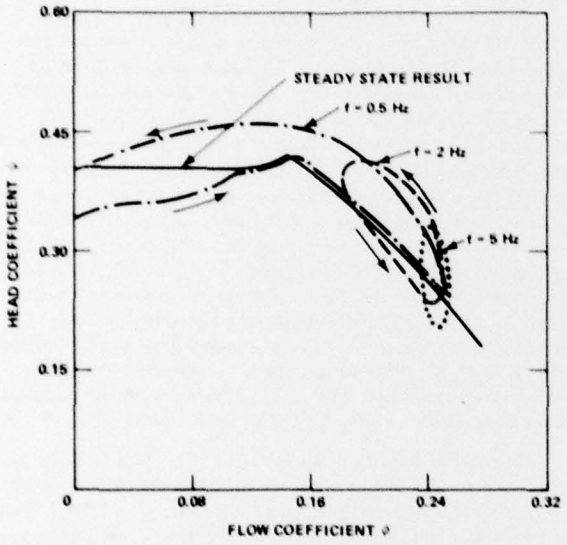


Fig. 2 – SES-100B Scale Model Lift Fan Dynamic Test Results

This paper presents the results of analyses conducted on the data obtained in the evaluation of the scale model centrifugal lift fan, and a method for predicting fan behavior in a dynamic environment. A computer simulation based on the method is verified using experimental data from the tests of the SES-100B, model fan, as well as a 1/4-scale model of the 2KSES lift fan. The analytical model of fan dynamic performance should be valuable in simulations of vertical motion of an SES or ACV in a seaway.

### Analysis of Fan Dynamic Data

Time histories of total and static pressure rise and air flow at frequencies of 0.5 Hz and 6 Hz are shown in Fig. 3. These data are illustrative of data obtained during the test of the 24-in. diameter SES-100B model cushion fan. Data were collected at fan speeds of 2560 and 3200 rpm. Where the wave forms were

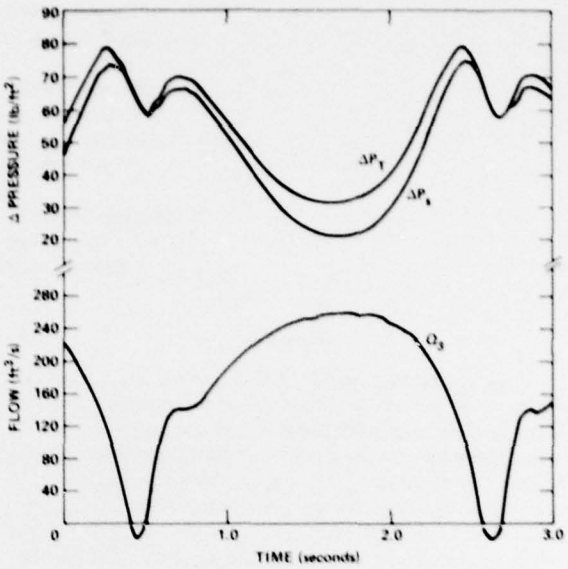


Fig. 3a – Test Data, 2560 rpm, 0.5 Hz

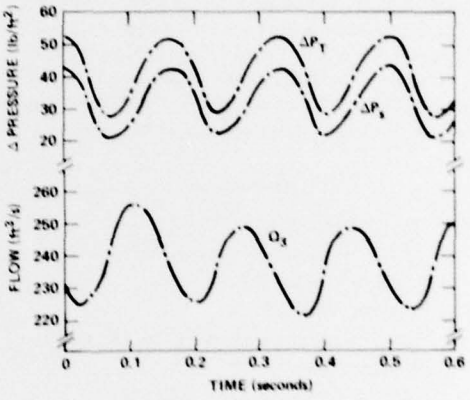


Fig. 3b – Test Data, 2560 rpm, 6 Hz

Fig. 3 – Total and Static Pressure and Flow Rate Time History

sufficiently sinusoidal, frequency response information in terms of the amplitude ratio and phase angle between fan flow and total pressure rise were evaluated. Examination of the frequency response information indicates that the amplitude ratio decreased and the phase angle increased as the excitation frequency was increased.

The response for a frequency of 0.5 and 1.0 Hz exhibited very large variations in flow and pressure, indicating extremely nonlinear operation. The operating point varied from nearly unrestricted flow to a backflow condition. At the high flow portions of each cycle the transient resulting from the nonlinearity decayed and linear operation was approached. A value of the phase shift was estimated in this operating region for both the 0.5 and 1.0 Hz data. At frequencies of 2 Hz and above, the wave forms were sufficiently sinusoidal to extract reliable frequency response data.

The amplitude ratios and phase angles of $\delta Q / \delta \Delta P_T$, determined from the time history data, are shown plotted as a

function of excitation frequency for fan speeds of 2560 and 3200 prm in Fig. 4. At each speed the data are compared to the frequency response characteristics of a simple first-order lag having the form:

$$\frac{\delta Q}{\delta \Delta P_T} = \frac{F_2}{1 + j(f/f_c)} \qquad (1)$$

The excellent correlation shown on the figure indicates that a first-order function adequately describes the dynamic characteristics of the fan within the test frequency range. The corner frequency $f_c$ appears to be slightly lower at the higher fan speed. The value of $F_2$ in Equation (1) is the inverse slope of the fan pressure-flow characteristic at the mean operating point.

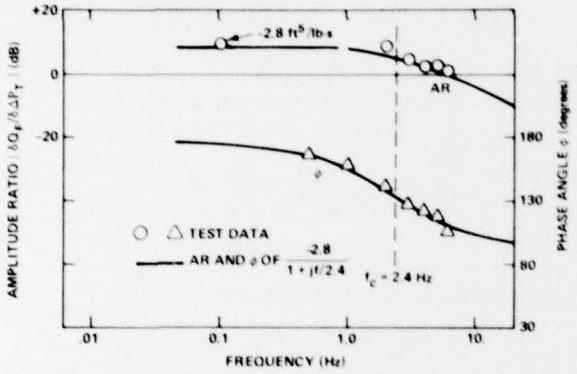


**Fig. 4a – Frequency Response Data at 2560 rpm**

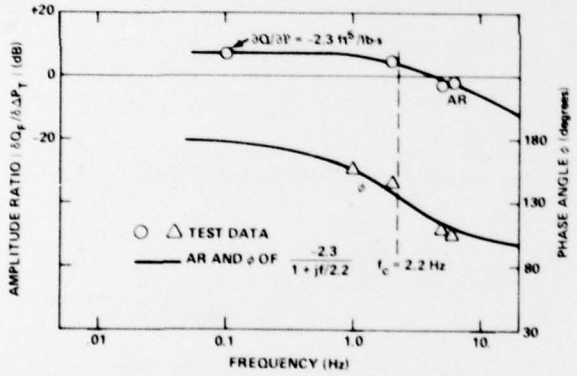


**Fig. 4b – Frequency Response Data at 3200 rpm**

**Fig. 4 – Bode Plot of SES-100B Scale Model Fan Response**

### Dynamic Analysis

An analysis was performed to identify the principal dynamic elements of the SES-100B cushion fan model system. Included in this were the following tasks:

1. Develop an analytical model which includes the principal dynamic elements of the fan test system.
2. Predict the behavior which each of the principal elements would produce under dynamic conditions.
3. Examine and compare the predicted behavior with that observed during the test program.
4. Eliminate those elements which do not produce the observed behavior.
5. Examine in greater detail the elements which result in system behavior similar to that observed during the test program, quantify parameters, and develop prediction methods.

A schematic diagram of the fan test system is shown in Fig. 5. The dynamic elements which are shown on the diagram are (1) the rotational inertia and torque-speed properties of the drive motor and fan, (2) the fluid dynamic properties of the air within the fan, and (3) the compliance and flow characteristics of the plenum. These elements were examined as possible causes of the observed fan behavior.

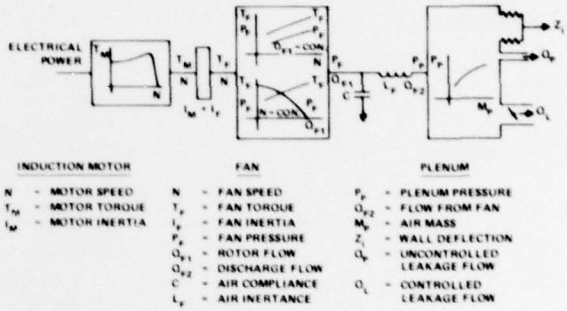


**Fig. 5 – Scale Model Fan System Schematic**

The equations which describe the system are listed below. As listed, they are in a somewhat simplified form which may be expanded in more detail, if required, as the particular elements are examined.

### System Equations

(See Fig. 5 for System Schematic)

#### Motor - Fan Rotational System

1. Motor Torque

$$T_M = f(N) \qquad (2)$$

2. Motor-Fan Speed

$$T_M - T_F = (I_M + I_F)\,\dot{\omega}_M \qquad (3)$$

3. Fan Torque

$$T_F = f(N, Q_F) \qquad (4)$$

Alternate Solution

$$T_F = f(N, \Delta P) \qquad (5)$$

#### Fan

1. Fan Discharge Pressure

$$\Delta P = f(N, Q_F) \qquad (6)$$

$$P_F = P_I + \Delta P \approx \Delta P \qquad (7)$$

Alternate Solution (with Fan compliance included)

$$Q_{F1} = f(N, \Delta P) \qquad (8)$$

$$\Delta P = P_F - P_I \approx P_F \qquad (9)$$

$$P_I = f(M_I) \qquad (10)$$

$$\dot{M}_I = \rho(Q_{F1} - Q_{F2}) \qquad (11)$$

2. Fan Discharge Flow

$$L_F \dot{Q}_{F2} = P_F - P_P \tag{12}$$

**Plenum**

1. Mass Accumulation

$$\dot{M}_P = \rho_P (Q_F - Q_P - Q_L) \tag{13}$$

2. Density

$$\rho_P = M_P / V_P \tag{14}$$

3. Pressure

$$P = \left[ \left( \frac{\rho_P}{\rho_{ATM}} \right)^{\gamma} - 1 \right] P_{ATM} \tag{15}$$

4. Volume

$$V_P = V_{PO} + \sum_{i=1}^{L} A_i Z_i \tag{16}$$

where:

$V_{PO}$ = undeformed volume
$A_i$ = effective area of wall section i
$Z_i$ = wall deflection of wall section i

$$P_P A_i = M_i \ddot{Z}_i + B_i \dot{Z}_i + K_i Z_i \tag{17}$$

5. Leakage Flows

$$Q_P = C_{DP} A_P \left[ \frac{2 P_P}{\rho_P} \right]^{1/2} \tag{18}$$

$$Q_L = C_{DL} A_L \left[ \frac{2 P_P}{\rho_P} \right]^{1/2} \tag{19}$$

The four primary differential equations which describe the dynamics of the system are Equations (3), (11), (12), and (13). Several more differential equations which describe the wall motion of the plenum would be necessary for a complete description. However, a knowledge of the dynamic characteristics of the plenum was not really necessary to the principal objective of the study, an understanding of the dynamic behavior of the fan. Since plenum pressure is approximately equal to the total pressure rise of the fan, total pressure rise data which were obtained during 100B testing were used directly.* Using the pressure rise data as an input to the fan model rather than a value obtained from a simulated plenum results in a much simpler, more accurate, and effective way of studying fan dynamic characteristics.

### Effects of Fan Speed Variations

Although speed variations were not regarded as a very likely cause of the fan's dynamic behavior, there were some questions as to the ability of the speed sensing system used in the test to record dynamic changes. Therefore, an analysis was performed to determine the effects of speed changes. The effects of speed variations were determined from the following linearized set of equations derived from the list of equations.

a. Motor Torque (from Equation (2))

$$\delta T_M = \frac{\partial T_M}{\partial \omega_M} \delta \omega_M = K_M \delta \omega_M \tag{20}$$

b. Fan Torque (from Equation (14))

$$\delta T_F = \frac{\partial T_F}{\partial \omega_M} \delta \omega_M + \frac{\partial T_F}{\partial Q_F} \delta Q_F \tag{21}$$

$$= K_1 \delta \omega_M + K_2 \delta Q_F$$

c. Motor-Fan Rotation (from Equation (3))

$$I_T \, \delta \dot{\omega}_M = \delta T_M - \delta T_F \tag{22}$$

d. Fan Discharge Pressure (neglecting the fan's fluid dynamic characteristics from Equation (6))

$$\delta P_F = \frac{\partial P_F}{\partial \omega_M} \delta \omega_M + \frac{\partial P_F}{\partial Q_F} \delta Q_F \tag{23}$$

$$= R_1 \delta \omega_M + R_2 \delta Q_F$$

Substituting Equations (20) and (21) into (22):

$$I_T \delta \dot{\omega}_M + (K_1 - K_M) \delta \omega_M + K_2 \delta Q_F = 0 \tag{24}$$

The following matrix equation in Laplace notation, formed from Equations (23) and (24), describes the motor fan system with fan discharge pressure as the excitation input.

$$\begin{bmatrix} I_T s + (K_1 - K_M) & K_2 \\ R_1 & R_2 \end{bmatrix} \begin{bmatrix} \delta \omega_M \\ \delta Q_F \end{bmatrix} = \begin{bmatrix} 0 \\ \delta P_F \end{bmatrix} \tag{25}$$

Solution of Equation (25) for fan flow $\delta Q_F$ in terms of discharge pressure $\delta P_F$ yields the following transfer function:

$$\frac{\delta Q_F}{\delta P_F} = \frac{(K_1 - K_M)}{R_2 (K_1 - K_M - R_1 K_2 / R_2)} \frac{\left[ \frac{I_T}{K_1 - K_M} s + 1 \right]}{\left[ \frac{I_T}{K_1 - K_M - R_1 K_2 / R_2} s + 1 \right]}$$

$$= K_R \frac{\left( \frac{s}{\omega_N} + 1 \right)}{\left( \frac{s}{\omega_D} + 1 \right)} \tag{26}$$

Since the discharge pressure perturbation $\delta P_F$ is essentially the same as the variation in fan pressure rise, the ratio $\delta Q_F / \delta P_F$ is the same function evaluated from the dynamic test data and plotted as a function of frequency in Fig. 4. Therefore, if variations in fan speed were the cause of the fan's dynamic behavior the transfer function of Equation (26), evaluated as a function of frequency, should yield a similar function. An examination of Equation (26) and its parameters indicates that

*It should be pointed out that the purpose of the plenum and discharge valve was to provide a variable backpressure environment for the fan. During testing, fan flow was observed to respond in a dynamic manner to the oscillatory backpressure. As the equations indicate, the fan will respond in the same manner to a given backpressure variation regardless of how the variation was produced.

it cannot result in frequency characteristics similar to those shown in Fig. 4.

At nominal operating conditions, the fan and motor parameters are such that: $K_1$ and $R_1 > 0$, $K_2 \geq 0$, and $R_2$ and $K_M < 0$. Therefore, $\omega_D \geq \omega_N$ indicates that the rotational system would introduce phase lead and an increase in amplitude ratio as a function of frequency rather than phase lag and attenuation as observed during the dynamic tests.

### Effects of the Fluid Dynamic Properties of the Air within the Fan

The air flowing within the fan possesses inertial and compliant properties which alternately store and return energy to the system under time varying conditions. The effects of these fluid dynamic properties on fan performance were examined. Inertia properties will be discussed first, then the combination of inertia and compliance.

The effects of air inertia were determined from a linearized small perturbation model of the fan. For small, very slowly varying changes where the effects of any dynamic characteristics are negligible, the change in pressure rise $\delta\Delta P$ is related to the change in flow $\delta Q_F$ as:

$$\delta\Delta P = \frac{\partial P}{\partial Q_F}\,\delta Q_F = \frac{1}{F_2}\,\delta Q_F \qquad (27)$$

Under normal operating conditions the pressure rise $\Delta P$ decreases with increasing flow $Q_F$ so that the partial derivative and the constant $F_2$, are negative. Equation (27) may also be written:

$$-\delta\Delta P = \delta P_I - \delta P_E = \frac{-1}{F_2}\,\delta Q_F \qquad (28)$$

where:

$P_I$ = fan inlet pressure

$P_E$ = fan discharge pressure

The constant $(-1/F_2)$ is analogous to a resistance between inlet and discharge.

The general effects of air inertia (inertance) on the behavior of the fan can be determined by applying Euler's equation to an undefined flow path representation of the fan.

$$\frac{\partial P}{\partial S} + \rho V\,\frac{\partial V}{\partial S} + \rho\,\frac{\partial V}{\partial t} = 0 \qquad (29)$$

where:

$P$ = pressure

$S$ = distance along flow path

$\rho$ = mass density

$V$ = velocity

$t$ = time

Assuming a constant mass flow rate $\dot{m}(t)$ along the flow path, the flow velocity $V$ is given by:

$$V(S, t) = \frac{\dot{m}(t)}{\rho(S, t)\,A(S)} \qquad (30)$$

In general, the mass density $\rho(S, t)$ varies with time in response to changes in back pressure, and also position due to the pressure rise of the fan. Substitution of Equation (30) into (29) gives:

$$\frac{\partial P}{\partial S} + \frac{\dot{m}(t)^2}{A(S)}\,\frac{\partial}{\partial S}\,\frac{1}{\rho(S, t)\,A(S)} + \frac{\rho(S, t)}{A(S)}\,\frac{\partial}{\partial t}\,\frac{\dot{m}(t)}{\rho(S, t)} = 0 \qquad (31)$$

The variations of both density $\rho$ and velocity $V$ with time and location prevent the separation of variables and a simple integration of Equation (31).

However, if density is also assumed constant along the flow path, then the volume flow rate is constant with respect to location and:

$$V(S, t) = \frac{\dot{m}(t)/\rho(t)}{A(S)} = \frac{Q_F(t)}{A(S)} \qquad (32)$$

Substitution of Equation (32) into (31) gives:

$$\frac{\partial P}{\partial S} + \frac{\rho Q(t)^2}{A(S)}\,\frac{\partial}{\partial S}\,\frac{1}{A(S)} + \frac{\rho \dot{Q}(t)}{A(S)} = 0 \qquad (33)$$

This equation can be integrated from inlet to outlet to give:

$$P_I - P_E = \frac{\rho Q(t)^2}{2}\left(\frac{1}{A_I^2} - \frac{1}{A_E^2}\right) + \rho \int_1^2 \frac{dS}{A(S)}\,\dot{Q}(t) \qquad (34)$$

The term involving the square of the flow divided by the square of the inlet and discharge area is simply the difference in dynamic pressures. The left side of the equation is the negative of the total pressure rise across the fan and Equation (34) may be written:

$$-\Delta P_T = P_{IT} - P_{ET} = \rho \int_1^2 \frac{dS}{A(S)}\,\dot{Q}_F(t) \qquad (35)$$

The assumption of constant density will generally provide a sufficiently accurate representation except for fans with a very high pressure rise. The constant density assumption is certainly adequate for the 100B subscale fan which has a pressure rise on the order of 100 lb/ft$^2$. The corresponding increase in density, assuming adiabatic compression is 3.4 percent.

For a pressure rise of 300 lb/ft$^2$ the density change is approximately 10 percent. However, the error resulting from a constant density assumption will be less than the change in density if the average density, rather than inlet or outlet density, is used in Equations (34) and (35). Therefore, a constant average density assumption is generally satisfactory for the dynamic analysis of most lift fans. Another factor which justifies the constant density approximation is the difficulty of accurately evaluating the integral of Equations (34) and (35).

Combination of the quasi-steady state characteristics given by Equation (28) with the dynamic characteristics of Equation (35), results in the following linearized, small perturbation description of the fan.

$$-\delta\Delta P_T = L_F\,\delta\dot{Q}_F(t) + \frac{1}{(-F_2)}\,\delta Q_F(t) \qquad (36)$$

where:

$$L_F = \rho \int_1^2 \frac{dS}{A(S)} = \text{inertance (lb-s}^2\text{/ft}^5\text{)} \qquad (37)$$

This equation describes a series circuit consisting of resistive and inertance elements. Laplace transforming and solving for fan flow in terms of total pressure rise yields:

$$\frac{\delta Q_F}{\delta \Delta P_T} = \frac{F_2}{-F_2 L_F s + 1} = \frac{F_2}{\frac{s}{\omega_c} + 1} \tag{38}$$

where:

$$\omega_c = \frac{-1}{F_2 L_F} = \text{corner frequency (rad/s)}$$

The first order dynamic characteristic of Equation (38) which results from inertance is of the form indicated by the fan test data as plotted in Fig. 4. In Fourier form Equation (38) becomes:

$$\frac{\delta Q_F}{\delta \Delta P_T} = \frac{F_2}{1 + j\frac{\omega}{\omega_c}} = \frac{F_2}{1 + j\frac{f}{f_c}} \tag{39}$$

where:

$$f_c = \frac{\omega_c}{2\pi} = \frac{1}{2\pi(-F_2)L_F}$$

Ohashi[3] performed an analytical and experimental study of the dynamic characteristics of turbopumps. An analytical model for the frequency response of a fan, derived from Ohashi's model, was utilized by Goldschmied and Wormley.[4] In the Ohashi paper, a model for oscillating flow through a cascade is developed. This is used to define the dynamic characteristics of a turbopump, which included the following three effects:

1. Oscillating flow through a variable area conduit,
2. Oscillating flow through the rotor cascade, and
3. Oscillating flow through the stator cascade.

The first of these is similar to the inertia effect identified as the primary contributor to the fan's dynamic properties as seen in the DTNSRDC test of the SES-100B model cushion fan. The latter two effects are mathematically expressed using the gamma function and the Gauss hypergeometric function. Ohashi goes on to present a simplified model of a turbopump which considers only the rotor and stator effects. Finally, he states that the time constant of a turbopump can be approximated by a first-order lag, which is the same type of function that was derived by analysis of the DTNSRDC test data.

Ohashi's paper concludes with a description of an experiment to measure the dynamic characteristics of a centrifugal pump. The comparison between his simplified theory and the experimental data showed that the experimental amplitude ratio decreased at a faster rate, and with a larger phase shift than the theory predicted. In fact, it appears that a more satisfactory fit between the experimental data and theory could be made with a first-order lag.

A comparison of the terms of Equation (39) with the numerical values determined from the curve fit of the test data given in Fig. 4 requires that:

$$-F_2 \approx 2.8 \tag{40}$$

and

$$L_F = \frac{1}{2\pi(-F_2)f_c} = \frac{1}{2\pi(2.8)(2.4)} = 0.0237 \tag{41}$$

Now, $F_2$ was defined as $\partial Q_F / \partial \Delta P_T$, which in turn was evaluated from the 2560 rpm fan characteristic to be approximately $-2.8$ ft$^3$/s/lb/ft$^2$. The inertance at 3200 rpm appears to be somewhat larger. A corner frequency $f_c$, of 2.2 Hz, as indicated in Fig. 4, and static fan slope of $-2.3$ ft$^3$/s/lb/ft$^2$ correspond to an inertance value 0.0315 (lb-s$^2$/ft$^5$). Although the reason for this apparent increase is not fully understood, it is believed to result from the higher flow and pressure at the higher speed. The volute is more uniformly filled with air which results in an increase in effective flow radius and path length. The increased density is also a contributor.

An evaluation of the fan inertance $L_F$ from Equation (37) is, in general, very difficult. The flow path is recognized as very complex and the flow itself probably not uniform and unidirectional at a given cross section. Therefore, a reasonable estimate of inertance is the best that can be obtained.

If the flow cross section A(S) was uniform then Equation (37) becomes the inertance for a uniform line $\ell$ units in length:

$$L_F = \frac{\rho \ell}{A} \text{ (lb-s}^2\text{/ft}^5\text{)} \tag{42}$$

A sketch of the fan volute is shown in Fig. 6. Considering the volute only, with an approximate length and average cross section of 9.5 ft and 1.5 ft$^2$, respectively an inertance of:

$$L_F = \frac{(0.0024)(9.5)}{1.5} = 0.0152 \text{ lb-s}^2\text{/ft}^5 \tag{43}$$

is obtained. In this representation the fact that all of the flow does not pass through the full length of the volute for which the inertance was calculated is offset by not considering the inertance of the air within the rotor and inlet.

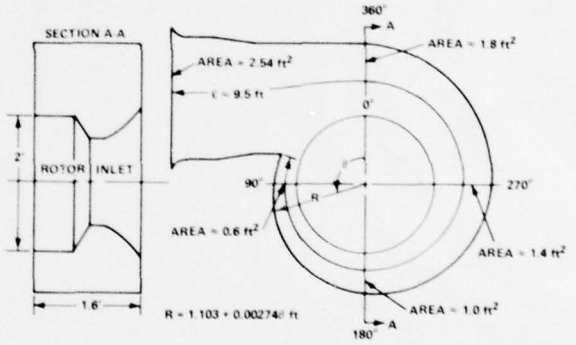


**Fig. 6 – SES-100B Scale Model Fan Geometry**

Another method of estimating the fan inertance is to determine the flow length based on the total volume of the fan and an average flow area. The total volume is on the order of 20 ft$^3$. Using an average flow area of 1.5 ft$^2$ the inertance is:

$$L_F = \frac{\rho V_F}{A^2} = \frac{(0.0024)(20)}{(1.5)^2} = 0.0213 \text{ lb-s}^2\text{/ft}^5 \tag{44}$$

A comparison of the two calculated inertance values with the value indicated by test data shows them to be of the same general magnitude. On the basis of this relatively close agreement between the geometrically calculated values and those determined from test data, it may be concluded that air inertia is a significant dynamic element and is the principal cause of the observed dynamic behavior.

The accurate determination of the inertance of a fan which has not been dynamically tested is difficult as previously indicated. However, for preliminary system analysis the methods

suggested will give an adequate representation. More accurate values can then be obtained through dynamic testing as illustrated here.

### Air Compliance

The effects of the compliance of the air within the fan can be evaluated through linearization and solution of fan Equations (8) through (12). Since the length of the flow path through the fan (<15 ft) is considerably shorter than a quarter wave length (47.5 ft), at a frequency of 6 Hz (the highest test frequency) a single lumped compliance representation is adequate. The linearized fan characteristic developed previously is:

$$\delta Q_{F1} = (-F_2)(\delta P_I - \delta P'_F) \tag{45}$$

This relation determines the flow into the fan. The discharge flow from the fan is determined by the inertance of the volute as:

$$\delta \dot{Q}_{F2} = (\delta P'_F - \delta P_F)/L_F \tag{46}$$

The rate of change of mass within the fan, which is proportional to the difference between the inlet and discharge flow, is then given by:

$$\delta M_F = \bar{\rho}_F (\delta Q_{F1} - \delta Q_{F2}) \tag{47}$$

where $\bar{\rho}_F$ is the nominal density within the fan.

Air density $\rho_F$ within the fan is related to the accumulated mass of air $M_F$ by:

$$\rho_F = M_F/V_F \tag{48}$$

and similarly for small changes:

$$\delta\rho_F = \delta M_F/V_F \tag{49}$$

where the volume of the fan $V_F$, small changes in fan pressure $\delta P'_F$, and density $\delta\rho_F$, are related by:

$$\frac{\delta P'_F + \bar{P}'_F}{\bar{P}_F} = \left(\frac{\delta\rho_F + \bar{\rho}_F}{\bar{\rho}_F}\right)^{\gamma} \tag{50}$$

and in linearized form by:

$$\delta P'_F = \frac{\partial \delta P'_F}{\partial \delta\rho_F}\,\delta\rho_F = \frac{\gamma \bar{P}'_F}{\bar{\rho}_F}\,\delta\rho_F \tag{51}$$

Taking the derivatives of Equations (49) and (51) and combining with Equation (47) the compliant properties of the fan are described as:

$$\delta \dot{P}'_F = \frac{(\delta Q_{F1} - \delta Q_{F2})}{C}$$

where:

$$C = \frac{V_F}{\gamma \bar{P}_F}\ (ft^5/lb)$$

Equations (45), (46), and (52) then describe the compliant and inertial characteristics of the fan to small perturbations. These three equations describe a system which is analogous to the simple electrical circuit shown in Fig. 7. Solution of the linearized equations yields the following transfer functions which give the flow rates $Q_{F1}$ and $Q_{F2}$ as a function of fan discharge pressure.

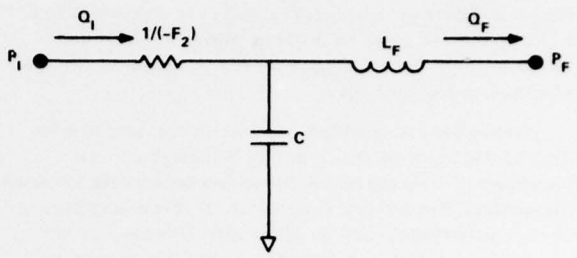


**Fig. 7 – Electrical Analog of Lift Fan System including Air Compliance**

$$\frac{\delta Q_{F1}}{\delta P_F} = \frac{F_2}{L_F C s^2 + (-F_2) L_F s + 1} \tag{53}$$

$$\frac{\delta Q_{F2}}{\delta P_F} = \frac{F_2\left(\frac{C}{-F_2}s + 1\right)}{L_F C s^2 + (-F_2) L_F s + 1} \tag{54}$$

For the SES-100B scale model fan, the volume $V_F$ is 20 $ft^3$, and C = 0.00644 $ft^5$/lb. Using values of $F_2$ and $L_F$ previously determined, the functions of Equations (53) and (54) become:

$$\frac{\delta Q_{F1}}{\delta P_F} = \frac{-2.8}{\left(\frac{s}{15.61} + 1\right)\left(\frac{s}{421} + 1\right)} \tag{55}$$

$$\frac{\delta Q_{F2}}{\delta P_f} = \frac{-2.8\left(\frac{s}{438} + 1\right)}{\left(\frac{s}{15.61} + 1\right)\left(\frac{s}{421} + 1\right)} \tag{56}$$

The compliance produces the high frequency form at 421 rad/s in Equations (55) and (56). This frequency is much higher than the lower frequency term which is attributed to inertance and, therefore, is of negligible significance with regard to the fan's dynamic characteristics within the test frequency range.

### Digital Computer Solution of Fan Performance

A time domain simulation was developed and programmed for solution on a digital computer. The inputs to the program include the steady state pressure-flow characteristic of the fan, the fan inertance geometry, and the discharge pressure time history. The simulation utilized a fourth-order Runge-Kutta integrator to integrate

$$\dot{Q}_F = \frac{A}{\rho \ell}(P'_F - P_p) \tag{57}$$

where

$P'_F = f(Q_F)$ (determined from the fan characteristic)

$P_p = P(t)$ (input from the time history test data)

$\rho = \left(\frac{P_{ATM} + P'_F}{P_{ATM}}\right)^{1/2} \rho_{ATM}$ (the calculated density of the air in the fan)

Inertance values based on the findings of the frequency response evaluation of the fan and the dynamic analysis were used in the simulation. Because the density is treated as a variable within the nonlinear simulation, the length to cross section ratio is input to the simulation rather than the inertance

value as indicated in Equations (37) and (42). A ratio ($\ell/A$) of 9.75 and 14.5 $ft^{-1}$ based on inertance values of 0.0237 and 0.0373 $lb-s^2/ft^5$ were simulated for the fan speeds of 2560 and 3200 rpm, respectively.

Comparisons of simulated response and test data at a fan speed of 2560 rpm are shown in Figs. 8 through 13. At frequencies of 2 Hz and above, correlation between the simulated and recorded flow response is excellent. Both the amplitude of the flow perturbations and the phase angle between flow and pressure rise are in close agreement. At these frequencies the perturbations are relatively small and operation remains on that portion of the fan characteristics where the slope is nearly constant. The system behavior is normal and hence the simulation completely describes the relationship between the pressure and flow perturbations.

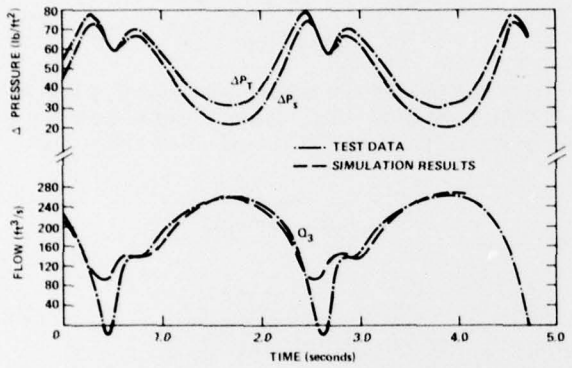


Fig. 8 – Correlation of Simulation Response with Test Data - Frequency = 0.5 Hz

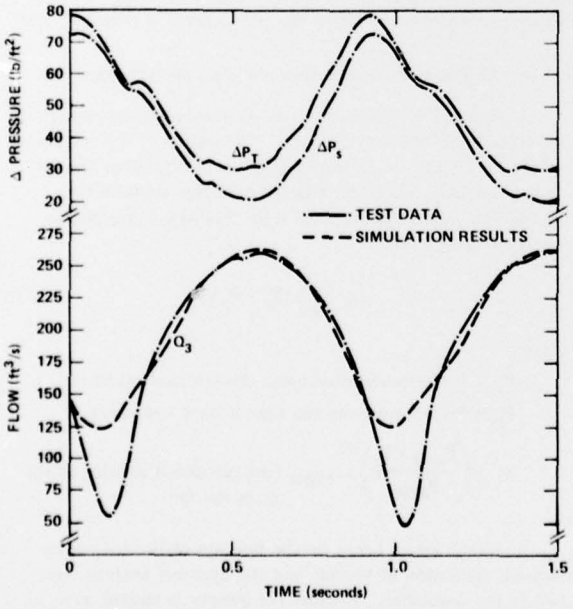


Fig. 9 – Correlation of Simulation Response with Test Data - Frequency = 1 Hz

At the lowest test frequencies (0.5 and 1.0 Hz shown on Figs. 8 and 9, respectively) the rotation of the discharge butterfly valve produces very large pressure and flow perturbations. Under these conditions the fan is operating within the stall region, and at cutoff during the 0.5 Hz perturbations, for a portion of the cycle. During the stall portion of the cycle it appears that the simulation is unable to determine the correct pressure-flow relationship. Although the flow predictions during the high flow portion of the cycle, the phase relationships, and general shape of the flow history appear correct, the deep troughs within the

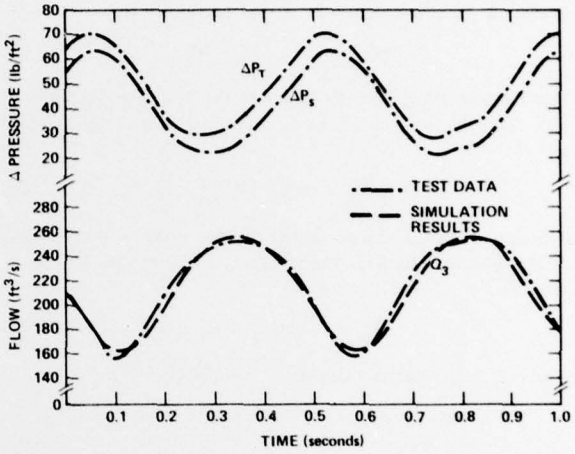


Fig. 10 – Correlation of Simulation Response with Test Data - Frequency = 2 Hz

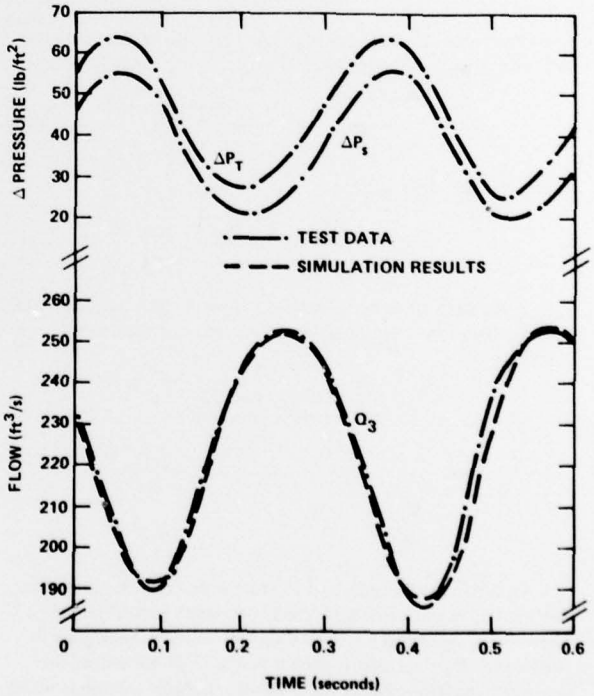


Fig. 11 – Correlation of Simulation Response with Test Data - Frequency = 3 Hz

flow trace are not achieved. The apparent inadequacy may rest in either the simulation or the pressure rise data which were used as the simulation excitation. During the tests of the SES-100B scale fan, it was noted that the rotation of the plenum butterfly valve was not steady at the low speeds corresponding to flow perturbation frequencies of 0.5 and 1.0 Hz, because at these speeds the drive system developed insufficient torque to counteract the aerodynamic moments which were acting on the valve.

Under these conditions, rapid pressure fluctuations occurred within the plenum and at the fan discharge, as shown in Fig. 8 where a double-peaked pressure transient was measured at low flows. It was postulated that the pressure transient that occurred under these conditions was actually more severe than was measured. With such an exaggerated pressure history, as indicated in Fig. 14, the simulated flow correlates very closely with test data.

It is also possible that fan inertance varies as a function of fan flow rate. Such a variation is suggested by the apparent difference in values observed at 2560 and 3200 rpm. Inertance values calculated from dynamic test data obtained at the two fan speeds are shown plotted as a function of flow rate in Fig. 15. Values determined from estimates of the fan's geometry are also shown for comparison. Extrapolation of the data obtained at the two fan speeds would indicate that very low values of inertance may exist at low flow rates.

If the effective inertance varies directly as a function of flow, then the extremely rapid flow changes which occur in the stall region would be possible with a less pronounced pressure fluctuation than indicated in Fig. 14. Although a variable inertance was not simulated, it is possible that such a variation is partially responsible, in addition to the previously discussed error in pressure rise data, for the discrepancy in low frequency simulated response. The variable inertance was not simulated

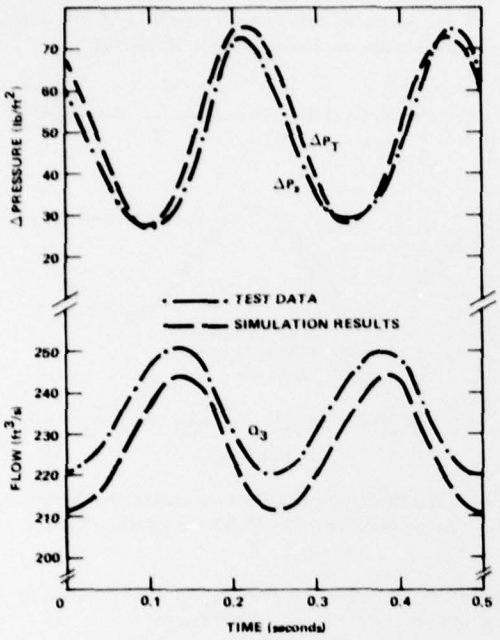


Fig. 12 – Correlation of Simulation Response with Test Data – Frequency = 4 Hz

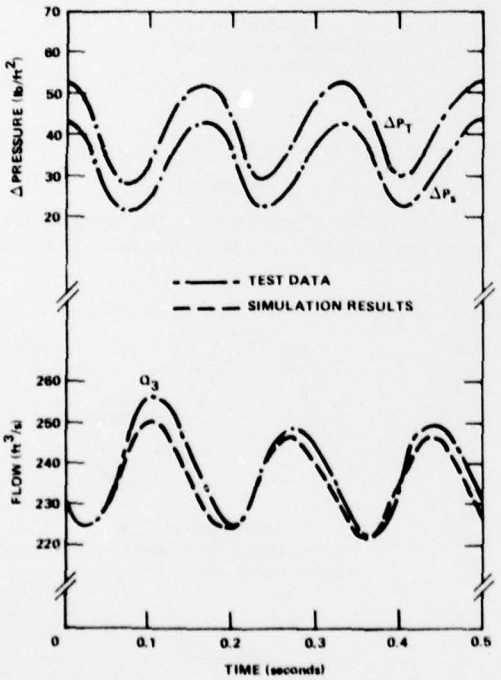


Fig. 13 – Correlation of Simulation Response with Test Data – Frequency = 6 Hz

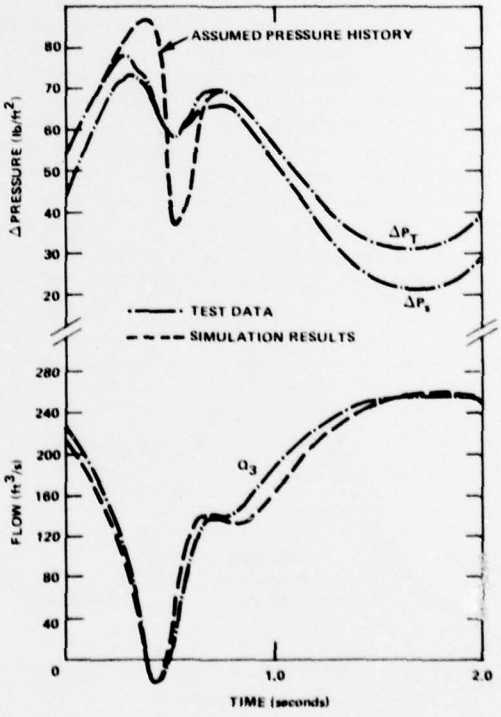


Fig. 14 – Simulation Response with Exaggerated Pressure Perturbation

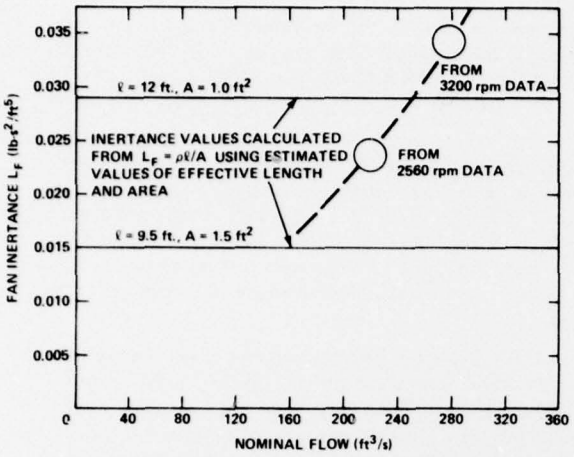


Fig. 15 – Fan Inertance Variation with Air Flow Rate

since values in the stall region would have been difficult to estimate without further dynamic testing within that region. Also, the value of such a simulation with regard to other fans would be minimal because the variation, which is a function of stall and flow separation characteristics, would undoubtedly be different for every fan, if it does exist.

The correlation between simulated response and test data indicates that the single lumped inertance representation is adequate for lift fan dynamic studies. An inertance value estimated from fan geometry is adequate for preliminary studies. More accurate values, possibly as a function of operating conditions, could be obtained from dynamic test results.

An evaluation similar to that conducted using the SES-100B scale cushion fan was subsequently conducted at DTNSRDC on a 24-in. diameter centrifugal fan that featured a servo-controlled variable geometry (VG) device to control the fan inlet flow and, ultimately, the plenum pressure. The fan was a double-inlet, single discharge configuration and was a 1/4-scale model of an early design of the lift fan for the 2KSES. Again the performance of the fan as measured during the test was compared with predictions generated using a digital computer simulation of the fan. In this case, the computer simulation was expanded so that the plenum pressure was calculated by integrating the air mass accumulation in the plenum, rather than using measured test data. A value for the fan inertance was determined for the fan volute geometry as before, and in addition, inclusion of the inertance of the plenum discharge valve was found to be necessary to achieve proper phase correlation between the valve area oscillation and the resultant change in the plenum pressure. Results of the comparison of plenum pressure test data and computer predictions are shown in Figs. 16 through 19.

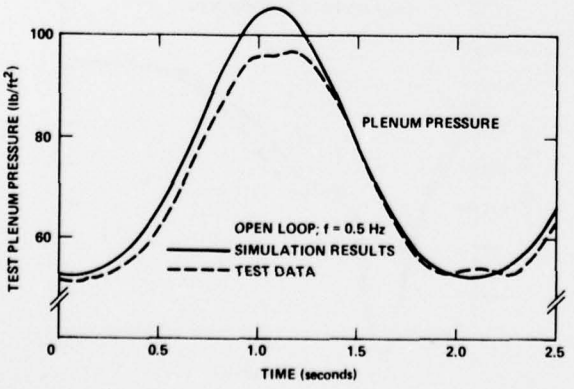


Fig. 16 – Correlation of Test Data and Simulation Response for a Fixed Geometry Fan Model - Frequency = 0.5 Hz

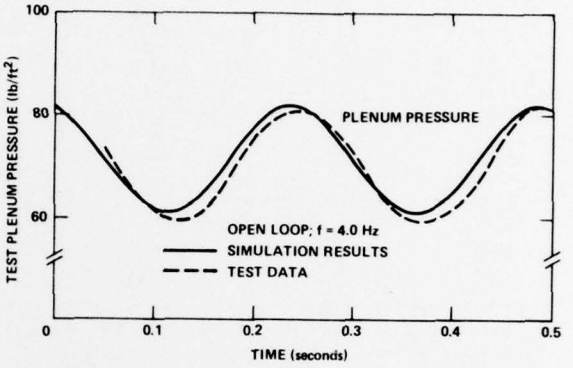


Fig. 17 – Correlation of Test Data and Simulation Response for a Fixed Geometry Fan Model - Frequency = 4 Hz

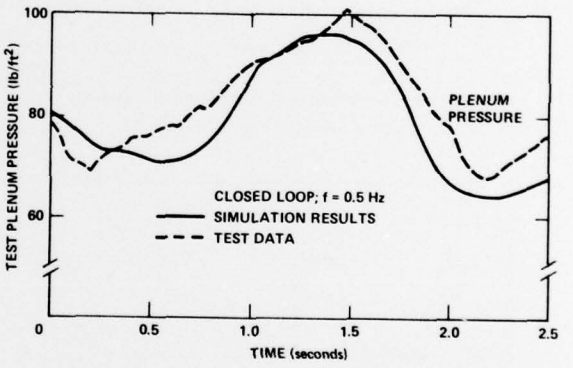


Fig. 18 – Correlation of Test Data and Simulation Response for a Fixed Geometry Fan Model - Frequency = 0.5 Hz

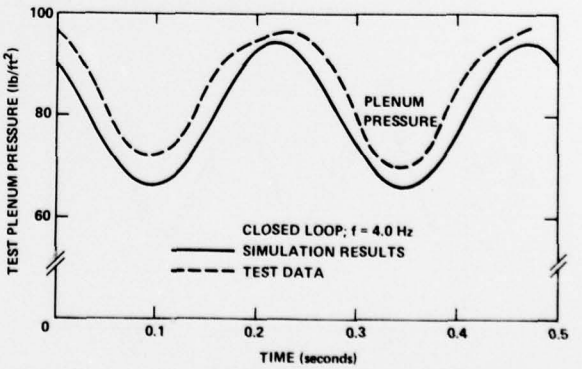


Fig. 19 – Correlation of Test Data and Simulation Response for a Fixed Geometry Fan Model - Frequency = 4 Hz

The comparison is shown at flow oscillation frequencies of 0.5 Hz and 4 Hz, for both the open loop (fixed geometry fan) and closed loop modes of fan operation. The comparison illustrates excellent correlation of the phase response during open loop operation. The simulation slightly overpredicted the peak pressure at low frequencies; at higher frequencies, the correlation of amplitude is excellent. When the fan was operated in the closed loop mode with variable geometry, the same comments apply to the comparison. In these cases, the simulation included the additional state variables necessary to describe the motion of the VG sleeve devices.

## Conclusions

The conclusions drawn from the above are summarized as follows:

1. Under dynamic air flow conditions, the lift fan response $\delta Q/\delta P$ can be represented by the transfer function of a first-order system with lag. At extremely low frequencies on the Bode plot, the amplitude ratio is flat and has a value corresponding to the negative inverse of the steady state fan slope $dP/dQ$. The phase angle in this case is 180 degrees. As the frequency is increased, the amplitude ratio decreases and the phase angle approaches 90 degrees. The corner frequency estimated from the test data was somewhat lower at the higher fan speed of the test data.

2. The dominant dynamic property responsible for the observed behavior of the fan is the fluid inertia, or inertance, of the air within the fan. A precise evaluation of the inertance of a fan from purely geometric considerations is difficult and analysis of test data is required for an accurate determination of the inertance properties. For most dynamic studies, however, sufficiently accurate analyses can be computed from fan geometry. The compliant properties, or capacitance, of the air within the test fan were found to be of negligible significance with regard to the observed behavior of the fan under dynamic flow conditions. This is also believed to be true for other lift fans. In general, these effects are of sufficient magnitude that they should be considered in air cushion lift system dynamic analyses.

3. A digital computer program has been developed to predict the performance of lift fans operating in an unsteady flow environment. Computer predictions of the fan flow rate have been correlated with measured test data for the SES-100 scale cushion fan and a 1/4-scale model of a 2KSES lift fan. Excellent agreement between the predicted and measured data is evident in the range of frequencies investigated.


## Acknowledgement

The work reported herein was performed under the sponsorship of the Surface Effect Ship Project Office (PMS-304). Their leadership and encouragement are gratefully acknowledged.


## References


1. Kaplan, P. and S. Davis, *"A Simplified Representation of the Vertical Plane Dynamics of SES Craft,"* AIAA Paper 74-314 (Feb 1974).

2. Durkin, J.M. and W.E. Langhi, *"An Investigation of the Performance of a Centrifugal Lift Fan Operating Against Sinusoidally Varying Back Pressure,"* Eighth Canadian Symposium on Air Cushion Technology, Toronto (Sep 1974).

3. Ohashi, H., *"Analytical and Experimental Study of Dynamic Characteristics of Turbopumps,"* NASA TN D-4298 (Apr 1968).

4. Goldschmied, F.R. and D.N. Wormley, *"Frequency Response of Blower/Duct/Plenum Fluid Systems,"* AIAA Journal of Hydronautics, Vol. 11, No. 1, pp. 18-27 (Jan 1977).

## INITIAL DISTRIBUTION

| Copies | |
|---|---|
| 1 | ARPA/Library |
| 1 | CHONR/461 |
| 1 | ONR SCI LIAISON GP/APO |
| 1 | NAV STRATEGIC SYS PROJ OFFICE<br>PM-1 |
| 1 | USNA/Library |
| 2 | NAVPGSCOL<br>1 Library<br>1 D. Layton/Aero Dept |
| 1 | NROTC & NAVADMINU, MIT |
| 1 | NSWC/Dahlgren<br>Tech Library |
| 1 | NSWC/White Oak<br>Tech Library |
| 1 | NUSC/Tech Library |
| 19 | NAVSEA<br>1 SEA 03B<br>1 SEA 032<br>1 SEA 09G32<br>16 PMS-304-141 |
| 1 | NISC |
| 3 | NAVSEC<br>1 SEC 6110<br>1 SEC 6114<br>1 SEC 6136 |
| 12 | DDC |
| 1 | Coast Guard HQ<br>Library/5-2 |

| Copies | |
|---|---|
| 1 | Marine Corps HQ/AX<br>A.L. Slafkosky/Sci Advisor |
| 2 | Maritime Admin<br>1 R&D Office<br>1 Div of Ship Design |
| 1 | Library of Congress<br>Science & Tech Div |
| 1 | AIAA/D. Staiger |
| 1 | SIT/Davidson Lab<br>J.P. Breslin |

### CENTER DISTRIBUTION

| Copies | Code | Name |
|---|---|---|
| 10 | 5214.1 | Reports Distribution |
| 1 | 522.1 | Library (C) |
| 1 | 522.2 | Library (A) |
| 1 | 522.3 | Aerodynamics Library |

PRECEDING PAGE BLANK

*U.S. GOVERNMENT PRINTING OFFICE:1978 261-250/070 1-3